Nitrosyl Derivatives of Diiron(I) Dithiolates Mimic the Structure and Lewis Acidity of the [FeFe]−Hydrogenase Active Site

ARTICLE *in* JOURNAL OF THE AMERICAN CHEMICAL SOCIETY · OCTOBER 2008

Impact Factor: 12.11 · DOI: 10.1021/ja802268p · Source: PubMed

Published in final edited form as:
J Am Chem Soc. 2008 September 10; 130(36): 12021–12030. doi:10.1021/ja802268p.

Nitrosyl Derivatives of Diiron(I) Dithiolates Mimic the Structure and Lewis Acidity of the FeFe-Hydrogenase Active Site

Matthew T. Olsen, **Maurizio Bruschi**, **Luca De Gioia**, **Thomas B. Rauchfuss**, and **Scott R. Wilson**

Department of Chemistry, University of Illinois at Urbana -- Champaign, Urbana, Illinois, 61801

Department of Biotechnology and Biosciences, University of Milano—Bicocca, Piazza della Scienza 1, 20126-Milan, Italy

Abstract

This study probes the impact of electronic asymmetry of diiron(I) dithiolato carbonyls. Treatment of $Fe_2(S_2C_nH_{2n})(CO)_{6-x}(PMe_3)_x$ compounds (n = 2, 3) with $NOBF_4$ gave the derivatives $[Fe_2(S_2C_nH_{2n})(CO)_{5-x}(PMe_3)_x(NO)]BF_4$ (x = 1, 2, 3) which are electronically unsymmetrical due to the presence of a single NO^+ ligand. Whereas the mono phosphine derivative is largely undistorted, the bis PMe_3 derivatives are distorted such that the CO ligand on the $Fe(CO)(PMe_3)(NO)^+$ subunit is semibridging. Two isomers of $[Fe_2(S_2C_3H_6)(CO)_3(PMe_3)_2(NO)]BF_4$ were characterized spectroscopically and crystallographically. Each isomer features electron-rich $[Fe(CO)_2PMe_3]$ and electrophilic $[Fe(CO)(PMe_3)(NO)]^+$ subunits. These species are in equilibrium with an unobserved isomer that reversibly binds CO (ΔH = −35 kJ/mol, ΔS = −139 J/mol•K) to give the symmetrical adduct $[Fe_2(S_2C_3H_6)(\mu\text{-}NO)(CO)_4(PMe_3)_2]BF_4$. In contrast to $Fe_2(S_2C_3H_6)(CO)_4(PMe_3)_2$, the bis (PMe_3) nitrosyls readily undergo CO-substitution to give the $(PMe_3)_3$ derivatives. The nitrosyl complexes reduce at potentials that are ~1 V milder than their carbonyl counterparts. DFT calculations, specifically NBO values, reinforce the electronic resemblance of the nitrosyl complexes with the corresponding mixed-valence diiron complexes. Unlike other diiron dithiolato carbonyls, these species undergo reversible reductions at mild conditions. The results show that the novel structural and chemical features associated with mixed valence diiron dithiolates – the so-called H_{ox} models - can be replicated in the absence of mixed-valency by introducing electronic asymmetry.

Introduction

Modeling of the hydrogenase enzymes complements biophysical studies, providing insights into the mechanism and spectroscopy relevant to this important family of biocatalysts.[1,2] The [FeFe]-hydrogenases are particularly attractive for modeling studies because the $Fe_2(SR)_2(CO)_{6-x}L_x$ core resembles well known organoiron complexes that are easily assembled with a variety of ligands and thiolates.[3,4] Variation of the coligands L and the thiolate SR offers the prospect for tuning the redox potentials and basicity of this diiron center. These variations in turn can affect the catalytic roperties of the diiron center, which undergoes three characteristic reactions – the reversible binding of CO, 1-electron redox, and the catalytic interconversion of protons and dihydrogen. Although hundreds of derivatives of $Fe_2(SR)_2(CO)_{6-x}L_x$ have been studied as models for the [FeFe]-hydrogenase, no $(Fe^I)_2$ compound to date exhibits the single most distinctive structural feature of the enzyme - the "rotated" nature of the distal iron center (Scheme 1). Previously we reported a method to induce

Correspondence to: Luca De Gioia, luca.degioia@unimib.it; Thomas B. Rauchfuss, rauchfuz@uiuc.edu.

rotation requiring strong Lewis acids, a highly basic diiron center, but resulting species were thermally unstable.[5]

The rotated structure is observed in the crystallography of the two active states, as revealed by the crystallographic studies of enzymes obtained from *C. pasteurianum* and *D. desulfuricans*.[6] The rotated geometry contrasts with the idealized C_{2v} structure and has recently been replicated in models for the H_{ox} state, which feature a mixedvalence diiron core.[7,8] The geometry of the diiron site in the H_{red} state is unclear – it is either rotated diiron(I) or diiron (II) core with a terminal hydride ligand.[9] From the mechanistic perspective, and relevant to understanding the hydrogenases as well as exploiting the diiron dithiolate platform for other applications, the rotated structure is of special significance because it provides a well-defined site for the binding of substrates.[1]

Many different types of ligands have been installed at one or more of the six terminal sites on the diiron dithiolate framework, including, in approximate order of their abundance, phosphines,[10] phosphites,[11] thioethers and bridging thiolates,[12,13] isocyanides,[14] carbenes,[15] arsines,[11] and alkenes.[16] Prior to this work, strong acceptor ligands had not been installed on the diiron(I) dithiolato platform, although electrophiles were found to add to the Fe-Fe bond.[17] In this work, we have examined the ability of NO^+ to alter the electronic structure of the diiron dithiolate carbonyls. As one of strongest acceptor ligands in inorganic chemistry,[18] NO^+ often forms complexes that are isoelectronic and isostructural with CO compounds.We show in this work, however, NO^+ forms diiron dithiolates that are not isostructural with the corresponding carbonyl complexes, and these nitrosyl complexes display enhanced Lewis acidity. Although iron nitrosyl thiolates have attracted intense interest,[19] the derivatives described below are novel. Closest to the present complexes are the Roussin esters $Fe_2(SR)_2(NO)_4$,[20] but substituted derivatives of these spin-paired 34e$^-$ diiron complexes have not been well developed.[21]

Results

Synthesis of $[Fe_2(S_2C_nH_{2n})(CO)_{5-x}(PMe_3)_x(NO)]BF_4$

Employing $NOBF_4$ as an NO^+ source, PMe_3-substituted diiron dithiolato carbonyls were found to readily undergo nitrosylation to afford monosubstituted products in good yields (Scheme 1). Thus, CH_2Cl_2 solutions of the complexes $Fe_2(S_2C_nH_{2n})(CO)_{6-x}(PMe_3)_x$ were found to react efficiently with suspensions of $NOBF^4$ over the course of hours at 0 °C for x = 1 and 2. In this way, we prepared $[Fe_2(S_2C_nH_{2n})(CO)_4(PMe_3)(NO)]BF_4$ for n = 2 (**1**) and 3 (**1'**) and $[Fe_2(S_2C_nH_{2n})(CO)_3(PMe_3)_2(NO)]BF_4$ for n = 2 (**2**) and 3 (**2'**) (eq 1). The IR spectra of **1** and **2** displayed νCO bands ~50 cm^{-1} higher in energy relative to their precursors. Each displayed a strong ν_{NO} band in the range ~1825 - 1760 cm^{-1}.

$$\begin{aligned} Fe_2(S_2C_nH_{2n})(CO)_{6-x}(PMe_3)_x + NOBF_4 \rightarrow\ & [Fe_2(S_2C_nH_{2n})(CO)_{5-x}(PMe_3)_x(NO)]BF_4 + CO \\ & [Fe_2(S_2C_2H_4)(CO)_4(PMe_3)(NO)]BF_4\,[\mathbf{1}]BF_4 \\ & [Fe_2(S_2C_3H_6)(CO)_4(PMe_3)(NO)]BF_4\,[\mathbf{1'}]BF_4 \\ & [Fe_2(S_2C_2H_4)(CO)_3(PMe_3)_2(NO)]BF_4\,[\mathbf{2}]BF_4 \\ & [Fe_2(S_2C_3H_6)(CO)_3(PMe_3)_2(NO)]BF_4\,[\mathbf{2'}]BF_4 \end{aligned} \quad (1)$$

Solutions of the mono and bisphosphines were stable for hours, eventually converting to mixtures containing the trisphosphine derivatives $[Fe_2(S_2C_nH_{2n})(CO)_2(PMe_3)_3(NO)]BF_4$ (see below) as well as other unidentified species.

Crystallographic Results

The structures **1**, **2**, **2'**, and **3'** were verified crystallographically. As expected, the $Fe^I{}_2(SR)_2$ core is complemented with six terminal ligands.[22] The iron-ligand distances in **1**, **2**, **2'**, and

3' are unremarkable, and carbonyl and nitrosyl ligands were distinguished by the Fe-NO distances, which were observed to be ~0.15 Å shorter than the Fe-CO distances (Figure 1–Figure 3).

The striking aspect of the structures is the distortion of the Fe_2L_6 framework from the usual[4] eclipsed quasi-C_{2v} geometry (Scheme 2). Especially for **2** and **2'**, the $Fe(CO)(PMe_3)(NO)^+$ subunits are rotated so as to orient a CO ligand into a semibridging position. This distortion is manifested in a more acute Fe^{CO}-Fe^{NO}-CO bond angle, Ψ, where Fe^{CO} and Fe^{NO} refers to the NO-free and NO-bearing iron atoms, respectively. Whereas mixed-valence diiron (I/II) dithiolato carbonyls display semi-bridging carbonyls with Ψ < 80° (see Table 1), for diiron(I) dithiolato carbonyls Ψ falls within the narrow range from 95 to 105°, e.g., for $Fe_2(S_2C_3H_6)(CO)_4(PMe_3)_2$ (103.6°).[23] For previously reported (NO^+-free) diiron dithiolates, this value varies only slightly (± 5°) depending on the size and chelating nature of the other ligands (see Table 1). Previously reported unsymmetrically substituted derivatives usually feature unremarkable structures.[24,25] One exception is the triphos complex.[22] Because of its rotated nature, the $Fe(CO)(PMe_3)(NO)^+$ center adopts an approximate T-shaped orientation.

Compound **1** crystallized with two molecules in its asymmetric unit, the Ψ values both being ~91° (Figure 1). These are less than typical (~100°) values but by the definition of Crabtree[26] correspond to terminal carbonyls. Otherwise, the structure is not unusual: the ligands are eclipsed and the $Fe(CO)_3$ subunit is unaffected.

Two separate rotamers of the bisphosphine propanedithiolate **2'** crystallized. Each is severely distorted. For one rotamer, labeled **2'^{ap}**, the phosphine on the $Fe(CO)_2(PMe_3)$ center occupies an apical site, and Ψ is 76° (Figure 2).

In the second rotamer, **2'^{ba}**, the phosphine ligand on the $Fe(CO)_2(PMe_3)$ center is basal, and the $Fe(CO)(PMe_3)(NO)^+$ center is even more distorted than in **2'^{ap}**. The shift of the PMe_3 ligand from the apical to the basal site on the $Fe(CO)_2PMe_3$ center induces the bridging CO ligand into a more symmetrical position. Two molecules were found in the asymmetric unit: Ψ = ~62° and 67°, i.e. these are bent semi-bridging carbonyls (Figure 3). The two distinct structures of **2'^{ba}** indicate some flexibility for the semi-bridging carbonyl parallel to the Fe-Fe vector. Because of the increased rotation of the $[Fe(CO)(PMe_3)(NO)]^+$ subunit (versus that seen in **2'^{ap}**), the vacant coordination site on Fe^{NO} is particularly open and more closely resembles the diiron coordination environment in the H_{ox} state and models thereof.[7,8] Although semi-bridging carbonyls are present in the solid state, a band for $\nu_{\mu-CO}$ is not apparent in the solution IR spectra of bulk samples of **2'** because **2'^{ba}** is a minority component. However, a $\nu_{\mu-CO}$ is observed in the solid-state IR spectrum of single crystals of **2'**.

The framework of ethanedithiolate **2** resembles that for **2'^{ap}** (see supplemental information). Only a single isomer was observed both in the solid state and in solution. The Ψ value is somewhat larger (~80°, i.e., FeCO is less bent) than for the propanedithiolate, consistent with the expected diminished steric influence of the smaller dithiolate.[5]

Given that two rotamers of **2'** crystallized, questions arose about the possibility that either **2'^{ap}** or **2'^{ba}** could be exceptional crystals that are not significantly represented in bulk samples. This issue was addressed through powder X-ray diffraction studies. Powder diffraction patterns for **2'^{ap}** and **2'^{ba}** were calculated from the single crystal data. The powder diffraction data for bulk samples were shown to consist of these two isomers as well as a third component. **2'^{ap}** was found to be the majority component, although calculations (below) suggest that **2'^{ba}** is ~3 kcal/mol lower in energy. That third component corresponds to species (one or more) obtained when single crystalline **2'** desolvates. The main point, however, is that of the solvates, polymorphs **2'^{ap}** and **2'^{ba}** are significant components of the solid mixture and are not statistical outliers.

Further substitution by phosphines occurs at the Fe^{NO} subunit to yield **3'** (see supporting information). Aside from a slightly distorted $Fe(PMe_3)_2(NO)^+$ subunit containing a Fe^{NO}-Fe^{CO}-P bond angle of 96°, the structure is typical.

DNMR Studies

Variable temperature NMR studies indicated that the propanedithiolate **2'** consists of two major isomers in solution, as anticipated from the crystallography. At 150 °C, the ^{31}P NMR spectrum consisted of two well resolved singlets (see supporting info). Upon cooling the sample, these peaks significantly broadened and decoalesced into a total of 4 peaks. Coalescence occurred at 25 and 10 °C, corresponding to the interconversion of **2'^{ap}** and **2'^{ba}** with an estimated activation energy in the range 51 – 52 kJ/mol. Below -60 °C, further splitting is observed due to the slow equilibration of the bridging propanedithiolate, as seen for non—nitrosylated $Fe_2(S_2C_3H_6)(CO)_4(PMe_3)_2$.[30]

The ^{31}P NMR spectrum of the ethanedithiolate **2** displayed only two singlets over the temperature range of 20 to −90 °C (Figure 4). Thus, it appears that only the propanedithiolate exists as energetically distinct rotamers.

Carbonylation of $[Fe_2(S_2C_nH_{2n})(CO)_3(PMe_3)_2(NO)]^+$

Unlike other diiron(I) dithiolates, **2'** and **2** are Lewis acidic - both reversibly add CO at low temperatures. In the IR spectrum of the adduct **2'**CO, ν_{NO} absorbs at 1513 cm^{-1}, about 200 cm^{-1} below the region for terminal nitrosyl ligands in this series. The spectra for the carbonylation exhibit isosbestic behavior, indicative of an equilibrium between two principal species (see Figure 5). Compounds **1** and **1'** did not display similar behaviour, however, ^{31}P NMR indicated that **3'** also formed an adduct with CO at low temperature (see Supplementary Information).

The IR spectra of **2'**CO are consistent with the presence of a bridging nitrosyl ligand. This assignment is supported by the low temperature ^{31}P NMR spectrum, which indicated equivalent phosphine ligands. Both isomers of **2'** formed the same adduct. The 200 cm^{-1} shift of the ν_{NO} band, also predicted by DFT calculations, is consistent with the relocation of the NO ligand from a terminal to a bridging position. Binding of CO by **2'** occurs with $\Delta H = -35$ kJ/mol and $\Delta S = -139$ J/mol•K, consistent with an associative process (eq 2, Figure 6). Despite the demonstrated affinity of **2'** for CO, solutions of **2'** did not appear to react with H_2. Furthermore no H-D exchange was observed when solutions of **2'** and H_2 were treated with MeOD in the presence of noncoordinating base.

Like **2'**, ethanedithiolate **2** displays a similar affinity toward CO. In a competition study, a solution that was equimolar in **2** and **2'** was treated with 1 atm of CO. Upon cooling to −80° C both CO adducts were observed, but **2'**CO was favored by ~7 fold relative to **2**CO. The adducts **2**CO and **2'**CO presumably occur as intermediates in the synthesis of **2'** from the reaction of NO^+ and $[Fe_2(S_2C_nH_{2n})(CO)_4(PMe_3)_2$.

Labeling with ^{13}CO has proven to be an effective tool to probe the carbonylation of models for H_{ox} and H_{ox} ^{CO},[31,32] but the present system is advantageous because the diamagnetism enabled analysis by ^{13}C NMR spectroscopy. Exposure of **2'** to ^{13}CO at −80 °C resulted primarily in a single isotopomers of **2'**CO and singly labeled **2'**. In **2'**^{13}CO, the label is proposed to be located at one of the two equivalent apical sites. The selectively labeled **2'** is proposed to arise by dissociation of ^{12}CO from one of these two equivalent apical sites. Upon thermal equilibration of the sample, the −80 °C spectrum displayed five ^{31}P-coupled doublets; two for

2'CO and three for the major isomer of **2'** (see supplementary information). If instead the ^{13}CO atmosphere was rigorously removed above the sample followed by thermal equilibration, the remaining carbonyls also became enriched.

When equimolar amounts of **1'** and **2'** were pressurized with ^{13}CO at −80 °C, the ^{31}P NMR spectra indicated carbonylation exclusively at **2'**, as expected since **1'** exhibits no Lewis acidity. Upon thermal equilibration, the ^{13}C NMR spectrum showed that **2'** alone was enriched. Similarly, when equimolar amounds of **2'** and **3'** were equilibrated under an atmosphere of ^{13}CO, enrichment was only observed at **2'**.

Reactions of PMe_3 with $[Fe_2(S_2C_nH_{2n})(CO)_3(PMe_3)_2(NO)]^+$

In contrast to the nucleophilicity of $Fe_2(S_2C_3H_6)(CO)_4(PMe_3)_2$, the nitrosyl compounds **2'** and **2** were found to be electrophilic. For example, **2'** is not visibly protonated by triflic acid. For example, they react readily with PMe_3 to afford the corresponding trisphosphines $[Fe_2(S_2C_nH_{2n})(CO)_2(PMe_3)_3(NO)]BF_4$, **3** and **3'**. Two intermediates for these conversions were detected by in-situ IR spectroscopy. An initial adduct was observed immediately upon the addition of the phosphine to a CH_2Cl_2 solution of the diphosphine complex at −80 °C. IR spectra showed that the ν_{NO} is most affected (Fig. 7). The IR spectrum resembles that for the above mentioned adducts **2'**CO and **2**CO, implicating the formation of a bridging NO complex. The ν_{NO} is ~25 cm^{-1} lower in energy.

The monophosphines **1** and **1'** were also found to readily undergo substitution by PMe_3 to give **2** and **2'**, respectively, as well as other nucleophiles (see supporting information). In these cases, IR measurements suggest that the nucleophile initially adds to the $Fe(CO)_3$ subunit via a metastable intermediate containing a bridging CO, although this aspect was not pursued.

Electrochemistry

Compounds **1**–**2** exhibit two one-electron reduction steps (Table 2), but they oxidize only at very positive potentials (>1.3 V versus Ag|AgCl). For **1** and **1'**, the first reductions are reversible, and the second reductions are only reversible at slow scan rates. Although $\Delta\nu_{NO}$ is much larger than $\Delta\nu_{CO}$, the effect of 1e reduction is smaller than that seen for the 1e reduction of mononuclear iron nitrosyls.[33] For **2'**, the first reduction is quasi-reversible ($i_{pa}/i_{pc} \approx 0.7$) at moderate scan rates (100 mV/s) and the second reduction is irreversible. The behavior of **2** is similar, although the first reduction is less reversible.

The reductions were determined to be 1—electron processes by comparing the i_p^a with the i_p^c of the oxidation of $Fe_2(S_2C_3H_6)(CO)_4$(dppv), which is known to be one— electron process.[34] Thus, in CH_2Cl_2 solution, compounds **1**—**3** are first reduced at the mild potentials of −0.36 (**1**) to −1.02 V (**3**) (potentials versus Ag|AgCl). Highlighting the electron—acceptor character of these nitrosyl complexes, the potentials for the second reduction of the diphosphine—derivatives **2**—**2'** are less negative than the *first* reduction step of the corresponding tetracarbonyl parents. Reduction of **2'** is about 0.1 *V* milder than that of **2**, indicating the expected effect of the dithiolate—bridge on the redox properties of the diiron derivatives.[5] In contrast to the behavior of compounds **1**—**2**, related complexes lacking NO^+ display reversible *oxidations* and a single poorly reversible reduction at highly negative potentials.[35,36]

DFT Calculations

DFT has accurately reproduced the experimental structure of **2'** (Figure S27, Supporting Information). The two isomers characterized by X-ray diffraction (**2'^{ba}** and **2'^{ap}**) correspond to the two most stable isomeric forms computed by DFT. However, several other isomers are within a few kcal/mol (see Supporting Information). To quantitatively evaluate the effect of the NO^+ ligand on the electronic structure of **2'^{ap}** and **2'^{ba}**, NBO charges (Table 3) have been

computed and compared to the corresponding values obtained for the optimized structures of the isoelectronic carbonyl, $Fe_2(S_2C_3H_6)(CO)_4(PMe_3)_2$ (ap and ba isomers). Related calculations for the oxidized species $[Fe_2(S_2C_3H_6)(CO)_4(PMe_3)_2]^+$ proved especially relevant. These species adopt "rotated" structures and are considered electronic models for the H_{ox} state of the active site.[34]

Although absolute values of NBO charges must be interpreted cautiously,[38] it is evident that the charge densities on the Fe atoms are far from formal oxidation states, reflecting the covalent character of the complex. Most importantly, the NBO charges on the Fe atoms in **2'^{ba}** and **2'^{ap}**, which formally are Fe(I)Fe(I) species, are more similar to the corresponding values calculated for the mixed-valence complex[7] $[Fe_2(S_2C_3H_6)(CO)_4(PMe_3)_2]^+$ than in the subferrous $Fe_2(S_2C_3H_6)(CO)_4(PMe_3)_2$ species. In particular, it can be concluded that the Fe^{NO} atom in $[Fe_2(S_2C_3H_6)(CO)_3(PMe_3)_2(NO)]^+$ (both isomers) have Fe(II)-like character. This observation conforms with the experimentally characterized Lewis acidity of the **2'** complex (see above) and its structural dissimilarity to Fe^IFe^I diiron dithiolates.[7]

Computed IR bands for the **2'** isomers (**2'^{ap}** and **2'^{ba}**) are collected in Table 4. The calculations are consistent with **2'^{ap}** being the major isomer in solution. Experimentally, signals corresponding to **2'^{ba}** are not observed, in part because ν_{NO} is intrinsically weaker and the ν_{CO} bands overlap with those for **2'^{ap}**. The lowest energy band always corresponds to ν_{NO}, whereas the other bands are assigned as ν_{CO}. Notably, moving from **2'^{ap}** to **2'^{ba}** the $\nu_{\mu\text{-}CO}$ band shifts by almost 100 cm^{-1}, due to the shortening of the C(O)—Fe^{CO} distance in **2'^{ba}** (2.78 versus 2.33 Å). The computed C(O)—Fe^{CO} distance in **2'^{ba}** could be underestimated due to the very flat potential energy surface corresponding to slight C(O)—Fe^{CO} distance modifications, as indicated also by the crystallographic results which range from 2.33 to 2.47 Å.

Calculations of the vibrational frequencies also supports the structure assigned to **2'**CO (see above). For example, the μ-NO group is calculated to be 1522 cm^{-1}, which reasonably matches the experimental value of 1513 cm^{-1}.

Regarding the structure of **2'**CO, DFT calculations indicate that the symmetrical μ-NO species is significantly more stable than other isomers (Figure 8), in agreement with the experimental evidence. Previous computational results from Schaefer and King indicate a preference for structures with bridging NO (relative to bridging CO) in electron-rich late transition metal complexes.[39] The enthalpy of carbonylation for **2'^{ba}**, −12.2 kcal/mol (Table 5), is also consistent with the experimental value.

Calculations predict that a high energy species (35 kcal/mol) features PMe_3 groups in apical positions with a *bent* NO ligand (Fe-N-O angle 123°). Interestingly, the Fe-Fe distance contracts to 2.591 Å. This *in silico* experiment demonstrates, in effect, the competition between bending of FeNO and Fe---Fe bonding. In other geometries, including the lowest energy species, the Fe---Fe distances are non-bonding: 2.987 (apical-PMe_3/μ-CO), 3.342 (equatorial-PMe_3/μ-CO), and 2.968 Å (equatorial-PMe_3/μ-NO).

We were surprised to observe bridging nitrosyl ligands in the adducts **2**CO and **2'**CO because the precursor complexes featured semi-bridging carbonyls that were expected to be occupy the bridging position. Calculations indicate enhanced stability for the adducts with μ-NO ligands and basal phosphines. Two isomerization pathways are plausible and very similar, involving turnstile rotations of the Fe^{NO} center. Only one isomer of CO adduct is observed. We did not consider alternative mechanisms involving the binding of CO directly to **2'^{ba}**, immediately followed by isomerization of NO into the bridging position, because the binding energies are unfavorable.

Discussion

The starting complexes in this work, species of the type $Fe_2(SR)_2(CO)_{6-x}L_x$, are well known, having been well developed even in the 1970's.[40] Because diiron(I) dithiolato carbonyls are structurally similar to the active site of the [FeFe]—hydrogenases, hundreds of derivatives have been described in recent years.[4] Although slight deviations from idealized symmetry are encountered with bulky or constraining ligands (see Table 1), this paper describes the first derivatives where Fe^IFe^I structures deviate strongly from the well established C_{2v} motif.[41,42] Our results demonstrate that electronic asymmetry imposed by ligands can cause very substantial geometric distortions otherwise induced by redox (Figure 9).[7,8] These distortions in turn impact the reactivity of these diiron compounds and further indicate the versatility of the $Fe_2(SR)_2(CO)_{6-x}L_x$ platform.[4]

The electronic asymmetry is particularly acute in the diphosphines $[Fe_2(S_2C_nH_{2n})(CO)_3(PMe_3)_2(NO)]^+$, wherein the $Fe(CO)(PMe_3)(NO)^+$ center is electrophilic and the $Fe(CO)_2(PMe_3)$ center is electron—rich. As seen previously,[5] the positioning of the central methylene group on the propanedithiolate accentuates the asymmetry by nonbonding interactions with ligands occupying the apical sites. As supported also by DFT calculations, the new compounds approximate the structure of the H_{ox} state of the diiron site of the [FeFe]-hydrogenases (Figure 10), possibly because these compounds simulate the electronic asymmetry of seen H_{ox} and its models.[43] Not only do $[Fe_2(S_2C_nH_{2n})(CO)_x(PMe_3)_2(NO)]^+$ (x = 3, 4) resemble the H_{ox}, the binding of CO gives a derivative that, like H_{ox}^{CO}, that is symmetrized. Recall that binding of CO to valence localized H_{ox} gives valence delocalized H_{ox}^{CO}.[7,31,34,44] Unlike the H_{ox}/H_{ox}^{CO} system and its models, which interconvert $33e^-/35e^-$ species, the $34e^-$ nitrosyl cations rearrange before forming the corresponding $36e^-$ adducts with CO.

Associated with their novel structures, the new nitrosyl derivatives exhibit properties rarely seen in related complexes:

1) *Lewis acidity*. Unlike the many previously reported 34e diiron(I) dithiolato complexes, the species $[Fe_2(S_2C_nH_{2n})(CO)_3(PMe_3)_2(NO)]^+$ are Lewis acidic.

2) *Interconversions involving μ-NO ligands*. The binding of CO provides a rare example of the interconversion of terminal and bridging NO ligands. Relatively few examples are known for complexes with μ—NO ligands,[46] but for dimetallic mixed CO-NO complexes NO bridges more often than CO.[39,47]

3) *Mild reduction potentials*. Nitrosyl derivatives of the diiron(I) dithiolates reduce at potentials approximately 1 V milder than for related complexes.[48] For example $Fe_2(S_2C_2H_4)(CO)_4(PMe_3)_2$ reduces at ~−1.5 V vs Ag|AgCl, whereas the nitrosyl derivatives reduce at ~ −0.5 V. The effect of replacing CO by NO^+ is equivalent to protonation of the related CO derivative.[36,49]

4) *Susceptibility toward ligand substitution*. Diiron(I) dithiolates resist polysubstitution by phosphine ligands, at least in the absence of chelate effects.[25,29] The presence of the nitrosyl allows the preparation of $[Fe_2(S_2C_3H_6)(CO)_2(PMe_3)_3(NO)]^+$. This finding further establishes that the resistance of $Fe_2(S_2C_3H_6)(CO)_4(PMe_3)_2$ toward substitution is not due to steric factors, but is the result of its diminished electrophilicity. The diiron center in the enzymes is bound to *three* terminal donor ligands: two cyanides and one 4Fe-4S cluster.[13]

5) *High rotational barriers*. The isolation of two rotamers separated by substantial (~12 kcal/mol) barriers, as in the case of **2'^{ap}** and **2'^{ba}**, is unprecedented within the chemistry of diiron (I) dithiolato carbonyls. High barriers to isomerization are implicated for mixed-valence diiron

dithiolates which also feature semibridging CO ligands.[34] A "turnstile" mechanism[42,50] is assumed to describe the interconversion of **2'^{ap}** and **2'^{ba}** (Scheme 4).

Experimental Section

Procedures and materials have recently been described.[25] $NOBF_4$ was sublimed at 200 °C (0.02 mm Hg).[51]

$[Fe_2(S_2C_2H_4)(CO)_4(PMe_3)(NO)]BF_4$, 1

At −30 °C, a mixture of 0.350 g (0.83 mmol) of $Fe_2(S_2C_2H_4)(CO)_5(PMe_3)$ and 0.095 g (0.81 mmol) of $NOBF_4$, in 20 mL of CH_2Cl_2 gave an intensely red solution over the course of 6 h. After concentrating the reaction to ~2 mL, the product precipitated upon addition of ~50 mL of hexanes and stirring for several minutes. The product was recrystallized by extraction into ~2 mL of CH_2Cl_2 followed by the addition of 50 mL of hexanes. Yield: 0.303 g (72%). Layering of a CH_2Cl_2 solution of **1** with hexanes afforded red single crystals after several days at −30 °C. 500 MHz ^{1}H NMR (CD_2Cl_2): δ 3.23 (ddd, J_{H-H} = 4.3, 8.2, 12.5, 1H, SCH_2), 3.07 (ddd, J_{H-H} = 4.5, 8.0, 17.3, 1H, SCH_2), 2.94 (ddd, J_{H-H} = 4.4, 8.0, 17.1, 1H, SCH_2), 2.88 (ddd, J_{H-H} = 4.4, 8.0, 17,1, 1H, SCH_2), 1.85 (d, J_{P-H} = 11.6, 9H, PMe_3). 202 MHz ^{31}P NMR (CD_2Cl_2, 20 °C): δ 21.4 (s). (CD_2Cl_2, −75 °C): δ 23.3 (s). IR (CH_2Cl_2): ν_{CO} = 2091, 2042; ν_{NO} = 1824 cm^{-1}. ESI-MS: *m/z* = 421.9 (M^+). Anal. Calcd for $C_9H_{13}BF_4Fe_2NO_5P_2S_2$ (found): C, 21.25 (20.96); H, 2.49 (2.49); N, 2.75 (2.69).

$[Fe_2(S_2C_3H_6)(CO)_4(PMe_3)(NO)]BF_4$, 1'

This compound was prepared as for **1** starting from 0.189 g (0.36 mmol) of $Fe_2(S_2C_3H_6)(CO)_5(PMe_3)$ and 0.048 g (0.41 mmol) of $NOBF_4$. Yield: 0.131 g (58%). 500 MHz ^{1}H NMR (CD_2Cl_2): δ 2.72 (m, 2H, SC*H*$_2$), 2.56 (m, 2H, SC*H*$_2$), 2.15 (m, 1H, C*H*$_2$), 2.03 (m, 1H, C*H*$_2$), 1.84 (d, J_{P-H} = 11.4, 9H, P*Me*$_3$). 202 MHz, ^{31}P NMR (CD_2Cl_2, 20 °C): 30.0 (s), (CD_2Cl_2, −80 °C): 32.3 (s), 24.9 (s). IR (CH_2Cl_2): ν_{CO} = 2089, 2036; ν_{NO} = 1813 cm^{-1}. ESI-MS: *m/z* = 421.9 (M^+). Anal. Calcd for $C_9H_{13}BF_4Fe_2NO_5P_2S_2$ (found): C, 22.97 (23.33); H, 2.89 (2.68); N, 2.68 (2.63).

$[Fe_2(S_2C_2H_4)(CO)_3(PMe_3)_2(NO)]BF4$, 2

To a mixture of 0.400 g (0.85 mmol) of $Fe_2(S_2C_2H_4)(CO)_4(PMe_3)_2$ and 0.100 g (0.86 mmol) of $NOBF_4$, cooled to 0 °C, was added 10 mL of CH_2Cl_2. After 3h, the dark brown-colored reaction mixture was concentrated *in vacuo* and precipitated upon addition of 50 mL hexanes. Recrystallization from 1:6 CH_2Cl_2:hexane mixtures provided analytically pure product. Yield: 0.435 g (91%). Layering of a CH_2Cl_2 solution of the product with hexanes followed by cooling at −30 °C, afforded deep red single crystals. ^{1}H NMR (CD_2Cl_2): δ 2.98 (m, 2H, SC*H*$_2$), 2.82 (m, 1H, SC*H*), 2.74 (m, 1H, SC*H*), 1.75 (d, J_{P-H} = 11.2, 9H, PMe_3), 1.69 (d, J_{P-H} = 9.8, PMe_3). ^{31}P NMR (CD_2Cl_2, 20 °C): δ 31.2 (bs), 28.4 (bs); (CD_2Cl_2, −90 °C): δ 34.5 (s), 34.0 (s). IR (CH_2Cl_2): ν_{CO} = 2035, 1980; ν_{NO} = 1793. ESI-MS: *m/z* = 470.1 (M^+). Anal. Calcd for $C_{11}H_{22}BF_4Fe_2NO_4P_2S_2$ (found): C, 23.73 (23.78); H, 3.98 (4.26); N, 2.53 (2.54).

$[Fe_2(S_2C_3H_6)(CO)_3(PMe_3)_2(NO)]BF_4$, 2'

The preparation was modeled after that for **2** from 0.504 g (1.05 mmol) of $Fe_2(S_2C_3H_6)(CO)_4(PMe_3)_2$ and 0.121 g (1.04 mmol) of $NOBF_4$. Yield: 0.382 g (64%). Layering of a CH_2Cl_2 solution of the product with hexanes followed by cooling to −30 °C, afforded dark brown needles. ^{1}H NMR (CD_2Cl_2): δ 2.58 (m, 2H, SC*H*$_2$), 2.45 (m, 2H, SC*H*$_2$), 1.10 (m, 2H, C*H*$_2$), 1.78 (d, J_{P-H} = 11.6, 9H, PMe_3), 1.72 (d, J_{P-H} = 10.1, 9H, PMe_3). ^{31}P NMR (CD_2Cl_2, 20 °C): δ 33.7 (bs), ~19 (bs, v. br); (CD_2Cl_2, −40 °C): 37.2 (s), 33.8 (s), 31.2 (s), 13.1 (s); (CD_2Cl_2, −90 °C): δ 41.4 (s), 38.7 (s), 36.4 (s), 34.0 (s), 32.0 (s), 14.6 (s), 13.4 (s). Integrations

indicate that the δ34.0 peak consists of two overlapping signals. IR (CH_2Cl_2): ν_{CO} = 2033, 1981, ν_{NO} = 1787. ESI-MS: *m/z* = 484.0 (M^+). Anal. Calcd for $C_{12}H_{24}BF_4Fe_2NO_4P_2S_2$ (found): C, 25.25 (25.07); H, 4.24 (4.20); N, 2.45 (2.40).

$[Fe_2(S_2C_3H_6)(CO)_2(PMe_3)_3(NO)]BF_4$, 3'

To a solution of 0.141 g (0.25 mmol) $[Fe_2(S_2C_3H_6)(CO)_3(PMe_3)_2(NO)]BF_4$ in 10 mL of CH_2Cl_2, cooled to −78 °C, was added 1.27 mL of a 0.193 M solution of PMe_3 (0.25 mmol) in CH_2Cl_2. The solution was warmed to room termperature and maintained at that temperature until all of the intermediate ($[Fe_2(S_2C_3H_6)(\mu\text{-}CO)(CO)_2(PMe_3)_3(NO)]BF_4$) had converted to **3'** (~ 2.5 h). The red product precipitated from solution upon addition of 50 mL of hexanes followed by removal of approximately 1/6 of the total volume *in vacuo*. Yield: 0.115 g (75%). Layering of a CH_2Cl_2 solution of the product with hexanes, followed by cooling this mixture to −30 °C, afforded dark red cubic single crystals after several days. ^{1}H NMR (CD_2Cl_2): δ 2.41 (m, 2H, SCH_2), 2.18 (m, 1H, C*H*$_2$), 2.11 (m, 2H, 2H, SC*H*$_2$), 1.76 (d, $J_{P\text{-}H}$ = 8.9, PMe_3), 1.71 (m, 1H, C*H*$_2$), 1.60 (s, 18H, PMe_3). ^{31}P NMR (CD_2Cl_2, 20 °C): δ 20.8 (s, 1P, Fe$(CO)_2(PMe_3)$), 6.4 (s, 2P, Fe$(PMe_3)_2(NO)$); (CD_2Cl_2, −40 °C): δ 20.8 (s, 1P, Fe$(CO)_2(PMe_3)$), 7.5 (s, 2P, Fe$(PMe_3)_2(NO)$). IR (CH_2Cl_2): ν_{CO} = 1991, 1939; ν_{NO} = 1755. ESI-MS: *m/z* = 532.3 (M^+). Anal. Calcd for $C_{14}H_{33}BF_4Fe_2NO_3P_3S_2$ (found): C, 27.17 (27.26); H, 4.24 (5.67); N, 2.26 (2.48). CV (CH_2Cl_2, vs Ag|AgCl): E_{pc} = −0.93, −1.49, E_{pa} = 1.02, 1.20 (reductions and oxidations were irreversible). During the synthesis of **3'**, in situ IR spectra (ReactIR 4000, Mettler Toledo) (CH_2Cl_2, −80 °C): ν_{CO} = 2034, 1984; ν_{NO} = 1486. IR (CH_2Cl_2, −45 °C): ν_{CO} = 1953; $\nu_{\mu\text{-}CO}$ = 1984; ν_{NO} = 1760.

CO Binding Experiments

In a typical experiment, onto ~8 mg of the diiron complex in a J. Young NMR tube was distilled 0.7 mL of CD*2*Cl*2*, and the solution was frozen in an isopentane/N*2* bath and the tube was evacuated. The tube was then pressurized with 1 atm of CO. After cooling to the appropriate temperature within the spectrometer, the reaction mixture was allowed to equilibrate until no significant changes were observed (typically ~30–60 min). The probe temperature was calibrated with a methanol standard.

[**2'**CO]BF_4: ^{31}P NMR (CD_2Cl_2, −80 °C): δ 21.2 (s, 1P). IR (CH_2Cl_2, −80 °C): ν_{CO} = 2038, 2003; ν_{NO} = 1513.

[**2**CO]BF_4: ^{31}P NMR (CD_2Cl_2, −80 °C): δ 22.1 (s, 1P). IR (CH_2Cl_2, −80 °C): ν_{CO} = 2038, 2011, 1999; ν_{NO} = 1498.

[**3'**CO]BF_4: (CD_2Cl_2, −80 °C): δ 19.5 (s, 1P), 19.3 (s, 1P), 18.2 (s, 1P), 18.1 (s, 2P), 17.5 (s, 1P). The low temperature ^{31}P NMR spectrum indicated that [**3'**CO]BF_4 consists of two isomers; one with 3 inequivalent phosphines, and the other containing 2 equivalent and 1 inequivalent phosphine.

Isotopic Labeling Experiments

J. Young NMR tubes were pressurized to ~0.3 atm of ^{13}CO, sealed, thawws in a CH_2Cl_2/N_2 slush bath and then immediately transferred to a spectrometer, where the probe was cooled to the appropriate temperature. A series of spectra were collected containing some combination of the following peaks: ^{13}C NMR (CD_2Cl_2, −80 °C): δ 222.2 (d, $J_{C\text{-}P}$ = 25.1, **2'**), 211.3 (d, $J_{C\text{-}P}$ = 12.0, **2'**), 210.8 (d, $J_{C\text{-}P}$ = 10.4, **2'**$(CO)_{ap}$), 205.9 (d, $J_{C\text{-}P}$ = 20.7, **2'**), 203.3 (d, $J_{C\text{-}P}$ = 16.5, **2'**$(CO)_{ba}$).

1. The initial spectrum at −80 °C showed a doublet at δ 210.8 and a weak signal at δ 205.9.

2. The sample was then warmed briefly by ejecting it followed after 5 s by reinjecting it into the −80 °C probe. The resultant spectrum showed signals at δ 210.8 and 205.9 of comparable intensity.
3. The sample was then ejected, warmed at 20 °C for ~5 min and then reinserting into the −80 °C probe, the spectrum feature all five signals listed above.
4. a. The sample was ejected, warmed to 20 °C for 5 min, and then vented to air. After cooling back to −80 °C, the spectrum showed peaks at δ 222.2, 211.3, and 205.9.
   b. Alternatively, the sample could be subjected to several freeze/pump/thaw cycles using a CH_2Cl_2/N_2 slush bath. The spectrum (−80 °C) consisted of a major signal at δ 205.9 and weaker signals at δ 222.2 and 211.3.

DNMR Measurements

With peaks at −30 °C labeled from left to right as A, B, C, and D: Coalescence of peaks A and C occurs at $T_c \approx 10$ °C with $\Delta\nu = 560$ Hz. The coalescence of peaks B and D occurs at $T_c \approx 25$ °C with $\Delta\nu = 2700$ Hz.

$$k_c = (\pi\Delta\nu)/(2^{1/2})$$
$$\Delta G^{\ddagger} = 19.14 T_c [10.32 + \log(T_c/k_c)]$$

These value correspond to the activation free energies of 51.4 and 52.4 kJ/mol [52]

X-ray Powder Diffraction

Powder diffraction patterns for **2**$^{\mathbf{ap}}$ and **2**$^{\mathbf{ba}}$ were calculated from the single crystal data using Topas, Version 3, by Bruker AXS.

DFT Calculations

DFT calculations were carried out using the BP86 functional[53] and a valence triple-ζ basis set with polarization on all atoms (TZVP),[54] a level of theory which has been found to give reliable results for analogous organometallic compounds.[55] Stationary points of the energy hypersurface have been located by means of energy gradient techniques and a full vibrational analysis has been carried out to further characterize each stationary point. Partial atomic charges have been computed according to the Natural Bond Orbital (NBO) scheme.[56]

Supplementary Material

Refer to Web version on PubMed Central for supplementary material.

Acknowledgement

This research was supported by the National Institutes of Health and the Petroleum Research Fund. MTO thanks the NIH Chemistry-Biology Interface program for support.

References

1. De Lacey AL, Fernández VM, Rousset M, Cammack R. Chem. Rev 2007;107:4304–4330. [PubMed: 17715982]
2. Fontecilla-Camps JC, Volbeda A, Cavazza C, Nicolet Y. Chem. Rev 2007;107:4273–4303. [PubMed: 17850165]Vignais PM, Billoud B. Chem. Rev 2007;107:4206–4272. [PubMed: 17927159]
3. Liu X, Ibrahim SK, Tard C, Pickett CJ. Coord. Chem. Rev 2005;249:1641–1652.
4. Hogarth, G. Comprehensive Organometallic Chemistry III. Mingos, RHCaDMP., editor. Elsevier: Amsterdam; 2007.

5. Justice AK, Zampella G, De Gioia L, Rauchfuss TB. Chem. Commun 2007:2019–2021.
6. Nicolet Y, Lemon BJ, Fontecilla-Camps JC, Peters JW. Trends Biochem. Sci 2000;25:138–143. [PubMed: 10694885]Pandey AS, Harris TV, Giles LJ, Peters JW, Szilagyi RK. J. Am. Chem. Soc 2008;130:4533–4540. [PubMed: 18324814]
7. Justice AK, Rauchfuss TB, Wilson SR. Angew. Chem., Int. Ed 2007;46:6152–6154.
8. Liu T, Darensbourg MY. J. Am. Chem. Soc 2007;129:7008–7009. [PubMed: 17497786]
9. van der Vlugt JI, Rauchfuss TB, Whaley CM, Wilson SR. J. Am. Chem. Soc 2005;127:16012–16013. [PubMed: 16287273]
10. Arabi MS, Mathieu R, Poilblanc RJ. Organomet. Chem 1979;177:199–209.
11. de Beer JA, Haines RJ. J. Organomet. Chem 1972;36:297–312.
12. Song L-C, Yang Z-Y, Bian H-Z, Hu Q-M. Organometallics 2004;23:3082–3084.
13. Tard C, Liu X, Ibrahim SK, Bruschi M, De Gioia L, Davies SC, Yang X, Wang L-S, Sawers G, Pickett CJ. Nature 2005;433:610–614. [PubMed: 15703741]
14. Nehring JL, Heinekey DM. Inorg. Chem 2003;42:4288–4292. [PubMed: 12844300]Boyke CA, Rauchfuss TB, Wilson SR, Rohmer M-M, Bénard M. J. Am. Chem. Soc 2004;126:15151–15160. [PubMed: 15548012]
15. Capon J-F, El Hassnaoui S, Gloaguen F, Schollhammer P, Talarmin J. Organometallics 2005;24:2020–2022.Tye JW, Lee J, Wang HW, Mejia-Rodriguez R, Reibenspies JH, Hall MB, Darensbourg MY. Inorg. Chem 2005;44:5550–5552. [PubMed: 16060601]
16. Lawrence JD, Li H, Rauchfuss TB. Chem. Commun 2001:1482–1483.
17. Arabi MS, Mathieu R, Poilblanc R. Inorg. Chim. Acta 1977;23:L17–L18.Arabi MS, Mathieu R, Poilblanc R. Inorg. Chim. Acta 1979;34:L207–L208.Bonnet JJ, Mathieu R, Poilblanc R, Ibers JA. J. Am. Chem. Soc 1979;101:7487–7496.
18. Mariusz MM, Artur MA. Organometallics 2007;25:6576–6580.Richter-Addo, GB.; Legzdins, P. Metal Nitrosyls. New York: Oxford University Press; 1992.
19. Butler AR, Megson IL. Chem. Rev 2002;102:1155–1165. [PubMed: 11942790]Wasser IM, de Vries S, Moënne-Loccoz P, Schröder I, Karlin KD. Chem. Rev 2002;102:1201–1234. [PubMed: 11942794] Tsai M-L, Liaw W-F. Inorg. Chem 2006;45:6583–6585. [PubMed: 16903707]Conradie J, Quarless DA Jr, Hsu H-F, Harrop TC, Lippard SJ, Koch SA, Ghosh A. J. Am. Chem. Soc 2007;129:10446–10456. [PubMed: 17685516]Harrop TC, Song D, Lippard SJ. J. Am. Chem. Soc 2006;128:3528–3529. [PubMed: 16536520]Harrop TC, Song D, Lippard SJ. J. Inorg. Biochem 2007;101:1730–1738. [PubMed: 17618690]
20. Rauchfuss TB, Weatherill TD. Inorg. Chem 1982;21:827–831.Conrado CL, Bourassa JL, Egler C, Wecksler S, Ford PC. Inorg. Chem 2003;42:2288–2293. [PubMed: 12665362]
21. Chen H-W, Lin C-W, Chen C-C, Yang L-B, Chiang M-H, Liaw W-F. Inorg. Chem 2005;44:3226–3232. [PubMed: 15847431]Lee C-M, Chen C-H, Chen H-W, Hsu J-L, Lee G-H, Liaw W-F. Inorg. Chem 2005;44:6670–6679. [PubMed: 16156625]
22. Adam FI, Hogarth G, Richards I, Sanchez BE. Dalton Trans 2007:2495–2498. [PubMed: 17563784]
23. Zhao X, Georgakaki IP, Miller ML, Yarbrough JC, Darensbourg MY. J. Am. Chem. Soc 2001;123:9710–9711. [PubMed: 11572707]
24. Duan LL, Wang M, Li P, Na Y, Wang N, Sun LC. Dalton Trans 2007:1277–1283. [PubMed: 17372642]
25. Justice AK, Zampella G, De Gioia L, Rauchfuss TB, van der Vlugt JI, Wilson SR. Inorg. Chem 2007;46:1655–1664. [PubMed: 17279743]
26. Crabtree RH, Lavin M. Inorg. Chem 1986;25:805–812.
27. Lyon EJ, Georgakaki IP, Reibenspies JH, Darensbourg MY. Angew. Chem., Int. Ed. Engl 1999;38:3178–3180. [PubMed: 10556894]
28. Li P, Wang M, He C, Li G, Liu X, Chen C, Åkermark B, Sun L. Eur. J. Inorg. Chem 2005:2506–2513.
29. Hogarth G, Richards I. Inorg. Chem. Commun 2007;10:66–70.
30. Georgakaki IP, Thomson LM, Lyon EJ, Hall MB, Darensbourg MY. Coord. Chem. Rev 2003:238–239. 255–266.

31. Justice AK, Nilges M, De Gioia L, Rauchfuss TB, Wilson SR, Zampella GJ. Am. Chem. Soc 2008;130:5293–5301.
32. Thomas CM, Liu T, Hall MB, Darensbourg MY. Chem. Commun 2008:1563–1565.
33. Sellmann D, Blum N, Heinemann FW, Hess BA. Chem. Eur. J 2001;7:1874–1880.Serres RG, Grapperhaus CA, Bothe E, Bill E, Weyhermuller T, Neese F, Wieghardt K. J. Am. Chem. Soc 2004;126:5138–5153. [PubMed: 15099097]
34. Justice AK, De Gioia L, Nilges MJ, Rauchfuss TB, Wilson SR, Zampella G. Inorg. Chem. 2008in press
35. Felton GAN, Vannucci AK, Chen J, Lockett LT, Okumura N, Petro BJ, Zakai UI, Evans DH, Glass RS, Lichtenberger DL. J. Am. Chem. Soc 2007;129:12521–12530. [PubMed: 17894491]Borg SJ, Behrsing T, Best SP, Razavet M, Liu X, Pickett CJ. J. Am. Chem. Soc 2004;126:16988–16999. [PubMed: 15612737]Borg SJ, Tye JW, Hall MB, Best SP. Inorg. Chem 2007;46:384–394. [PubMed: 17279816]
36. Gloaguen F, Lawrence JD, Rauchfuss TB, Bénard M, Rohmer M-M. Inorg. Chem 2002;41:6573–6582. [PubMed: 12470052]
37. Mejia-Rodriguez R, Chong D, Reibenspies JH, Soriaga MP, Darensbourg MY. J. Am. Chem. Soc 2004;126:12004–12014. [PubMed: 15382935]
38. Reed AE, Curtiss LA, Weinhold F. Chem. Rev 1988;88:899–926.
39. Wang H, Xie Y, King RB, Schaefer HF III. Inorg. Chem 2008;46:1836–1847. [PubMed: 17269763]
40. Zhao X, Georgakaki IP, Miller ML, Mejia-Rodriguez R, Chiang C-Y, Darensbourg MY. Inorg. Chem 2002;41:3917–3928. [PubMed: 12132916]Fauvel K, Mathieu R, Poilblanc R. Inorg. Chem 1976;15:976–978.
41. Dahl LF, Wei CH. Inorg. Chem 1963;2:328–333.
42. Winter A, Zsolnai L, Huttner GZ. Naturforsch 1982;37b:1430–1436.
43. Nicolet Y, Piras C, Legrand P, Hatchikian CE, Fontecilla-Camps JC. Structure 1999;7:13–23. [PubMed: 10368269]
44. Silakov A, Reijerse EJ, Albracht SPJ, Hatchikian EC, Lubitz W. J. Am. Chem. Soc 2007;129:11447–11458. [PubMed: 17722921]
45. Peters JW, Lanzilotta WN, Lemon BJ, Seefeldt LC. Science 1998;282:1853–1858. [PubMed: 9836629]
46. Paul PP, Tyeklar Z, Farooq A, Karlin KD, Liu S, Zubieta J. J. Am. Chem. Soc 1990;112:2430–2432.
47. Hayton TW, Legzdins P, Sharp WB. Chem. Rev 2002;102:935–991. [PubMed: 11942784]
48. Cheah MH, Borg SJ, Best SP. Inorg. Chem 2007;46:1741–1750. [PubMed: 17256930]
49. Gloaguen F, Lawrence JD, Rauchfuss TB. J. Am. Chem. Soc 2001;123:9476–9477. [PubMed: 11562244]
50. Adams RD, Cotton FA, Cullen WR, Hunter DL, Mihichuk L. Inorg. Chem 1975;14:1395–1399.Lyon EJ, Georgakaki IP, Reibenspies JH, Darensbourg MY. J. Am. Chem. Soc 2001;123:3268–3278. [PubMed: 11457062]
51. Mocella MT, Okamoto MS, Barefield EK. Syn. React. Inorg. Metal-Org. Chem 1974;4:69–90.
52. Nelson, JH. Nuclear Magnetic Resonance Spectroscopy. NY: Prentice Hall; 2003.
53. Becke AD. J. Chem. Phys 1986;84:4524–4529.Perdew JP. P. Phys. Rev 1986;B33:8882.
54. Schaefer A, Huber C, Ahlrichs R. J. Chem. Phys 1994;100:5829–5835.
55. Niu S, Hall MB. Chem. Rev 2000;100:353. [PubMed: 11749240]Bruschi M, Zampella G, Fantucci P, De Gioia L. Coord. Chem. Rev 2005;249:1620.Siegbahn PEM, Tye JW, Hall MB. Chem. Rev 2007;107:4414–4435. [PubMed: 17927160]
56. Reed AE, Weinstock RB, Weinhold F. J. Chem. Phys 1985;83:735–746.

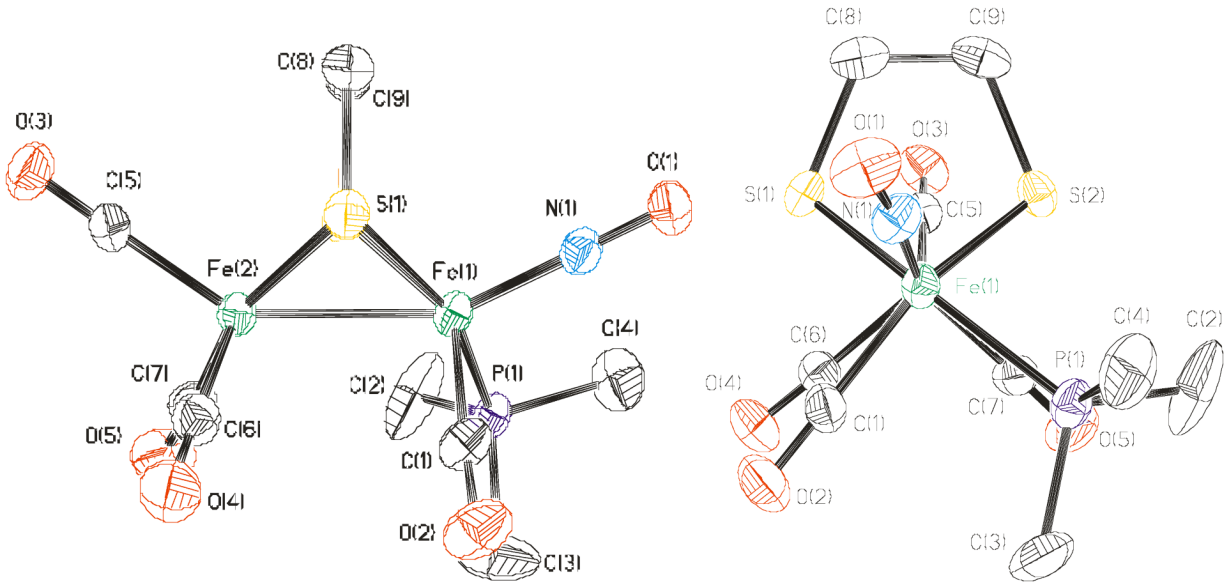

Figure 1.

Structure of **1** with thermal ellipsoids set at 35%. Disordered anions and hydrogen atoms have been omitted for clarity. Key bond distances (Å): Fe1-Fe2, 2.5529(9); Fe1-N1, 1.669(4), 1.67; Fe1-P1, 2.2971(13); Fe1-C1, 1.821(5); Fe2-C5, 1.804(4); Fe2-C6, 1.804(5); Fe2-C7: 1.794(5).

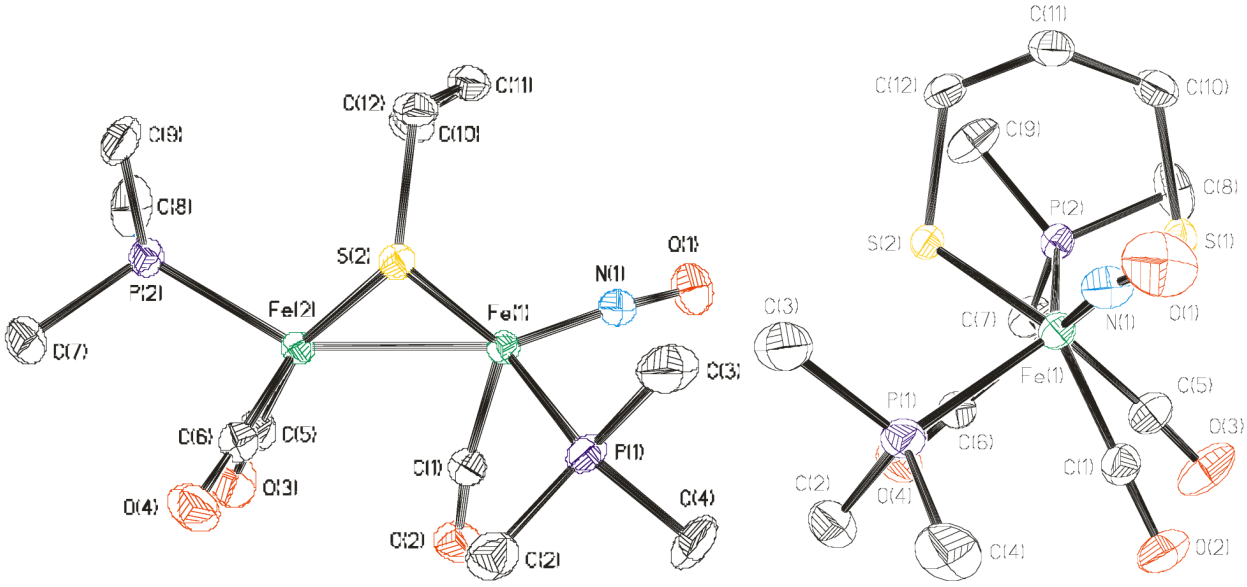

Figure 2.

Structure of **2'^{ap}** with thermal ellipsoids set at 35%. Side-on (left) and end-on (right) views. Hydrogen atoms, disordered methyl groups on P2, the anion, and solvate have been omitted for clarity. Key bond distances (Å): Fe1-Fe2, 2.5806(5); Fe1-N1, 1.648(3); Fe1-P1, 2.2622(8); Fe1-C1, 1.794(3); Fe2-C5, 1.778(3); Fe2-C6, 1.777(3); Fe2-P2, 2.2231(8).

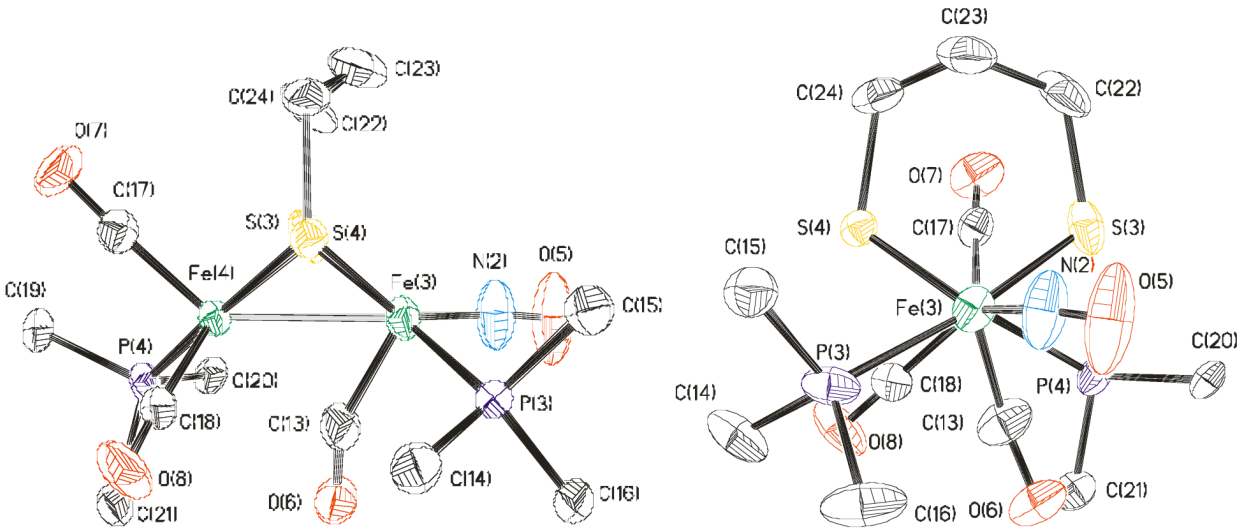

Figure 3.

Structure of **2'ba** with thermal ellipsoids set at 35%. Of the two molecules in the asymmetric unit, the one with the smaller Ψ value (62.1°) is displayed. Side—on (left) and end—on (right) views. Hydrogen atoms, disordered methyl groups on P4, disorder in C13 and O6, anion, and solvate have been omitted for clarity. Key bond distances (Å): Fe3-Fe4: 2.5433(12), Fe3-N2: 1.616(6), Fe3-P3: 2.253(2), Fe3-C13: 1.778(9), Fe4-C13: 2.323(9), Fe4-C17: 1.747(7), Fe4-C18: 1.786(7), Fe4-P4: 2.273(4).

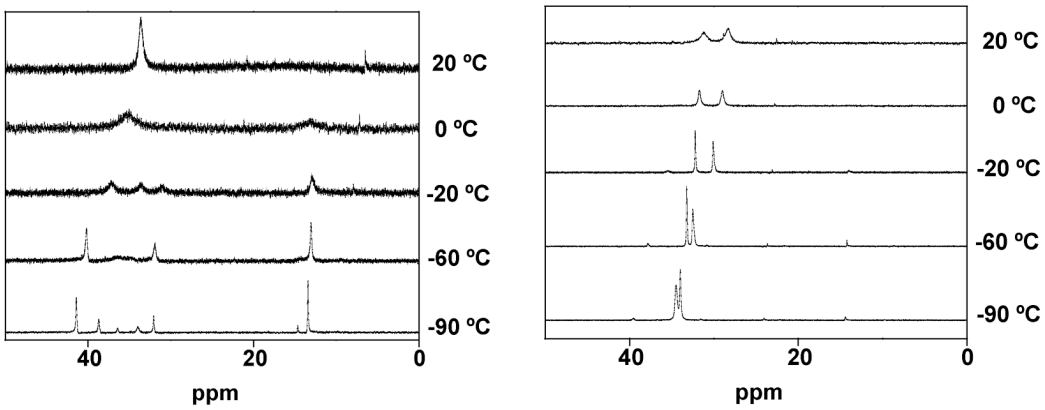

Figure 4.
202 MHz ^{31}P NMR spectra of **2'** (left) and **2** (right) at various temperatures (CD_2Cl_2 solutions).

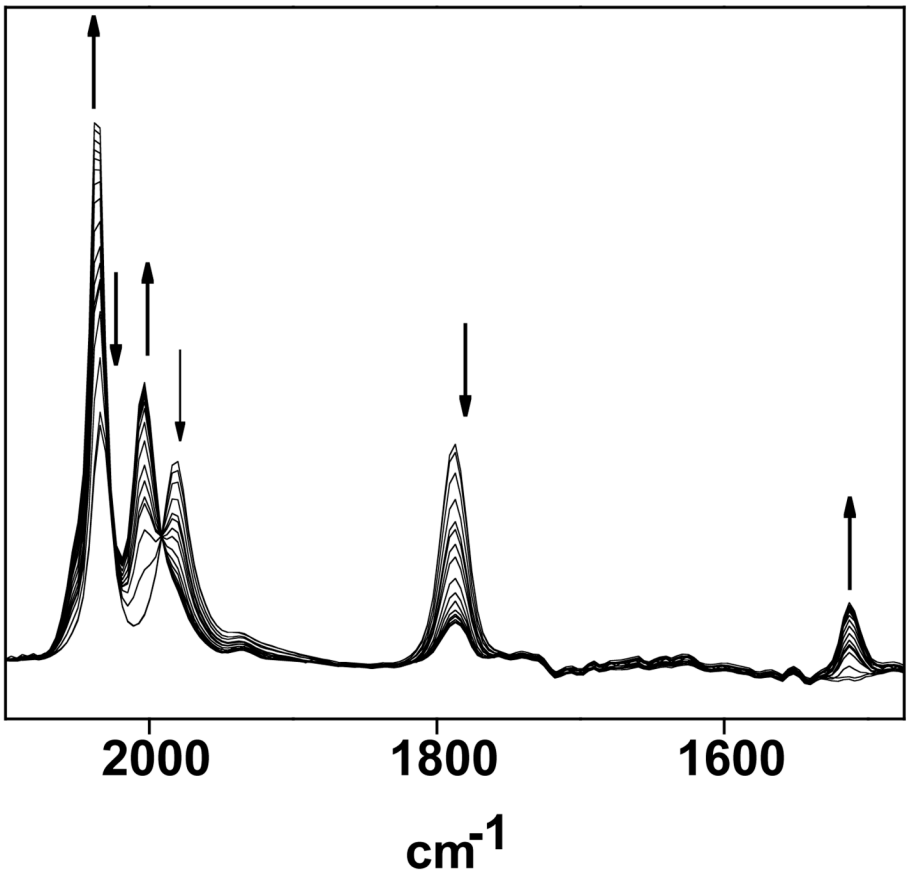

Figure 5.
IR spectra recorded at intervals over the course of 10 min for the carbonylation of **2'** (CH_2Cl_2 solution, −80 °C). Notice the diminution of the 1797s cm^{-1} band for **2'** and the concomitant appearance of the band at 1513 cm^{-1} in **2'**CO assigned to $\nu_{\mu\text{-NO}}$.

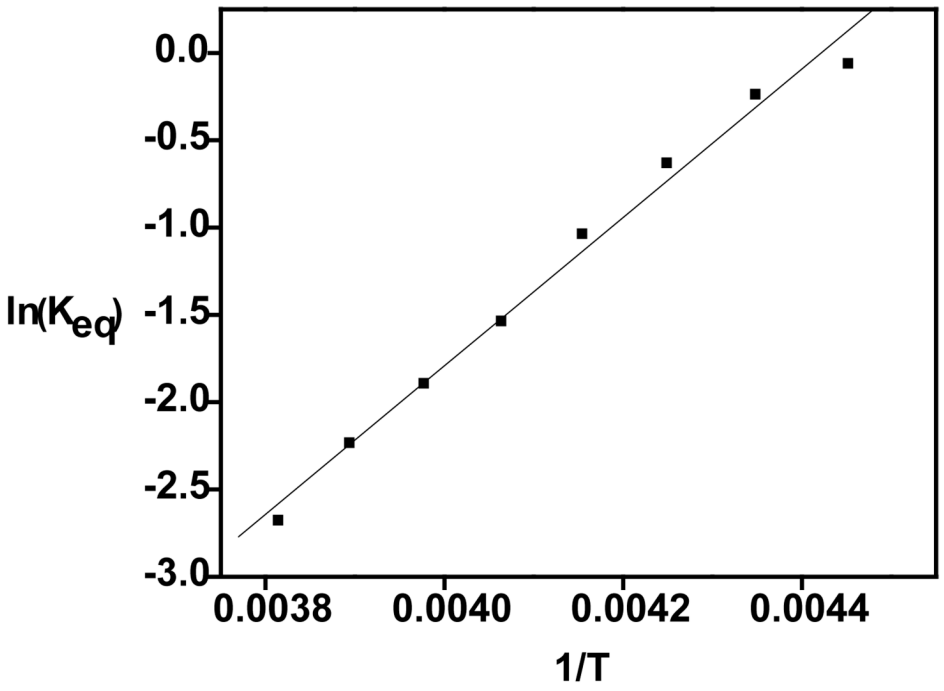

Figure 6.
Plot of ln(K_{eq}) vs 1/T (K) for 0.022 M **2'** (CH_2Cl_2) under 1 atm CO.

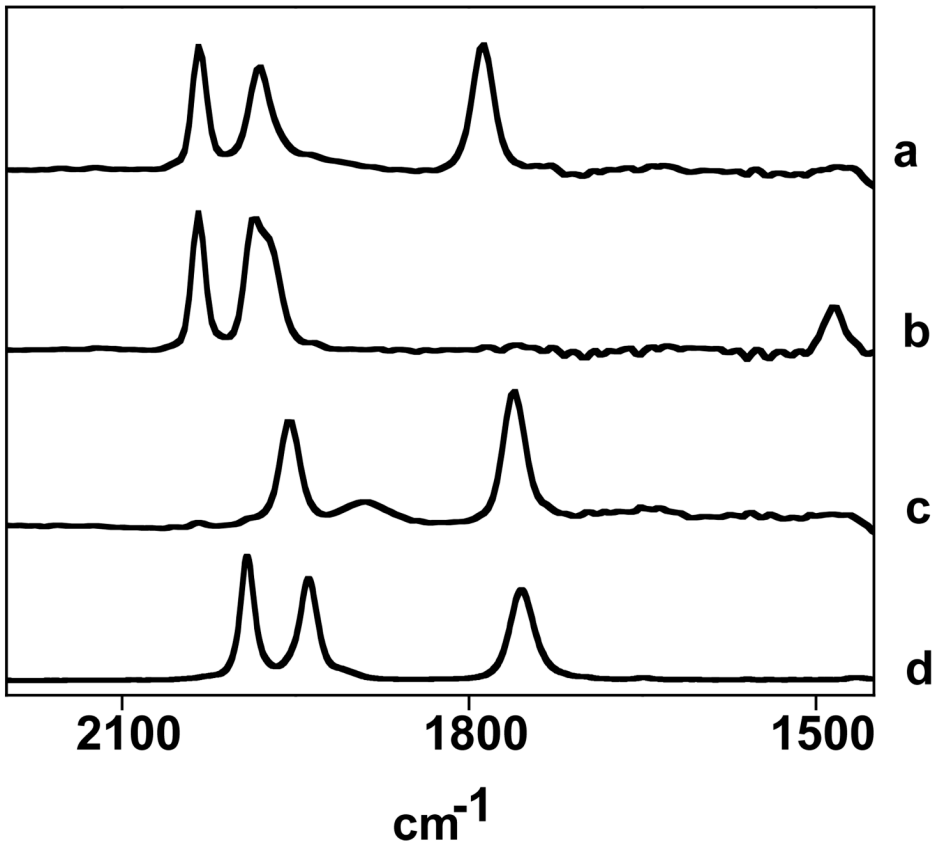

Figure 7.
IR spectra of **2'** (CH_2Cl_2 solution) at −78 °C (a), following the addition of one equiv of PMe_3 (b), upon warming to −45 °C for 10 min. (c), and upon warming to room temperature for 3 h (d). For peak maxima, see Experimental Section.

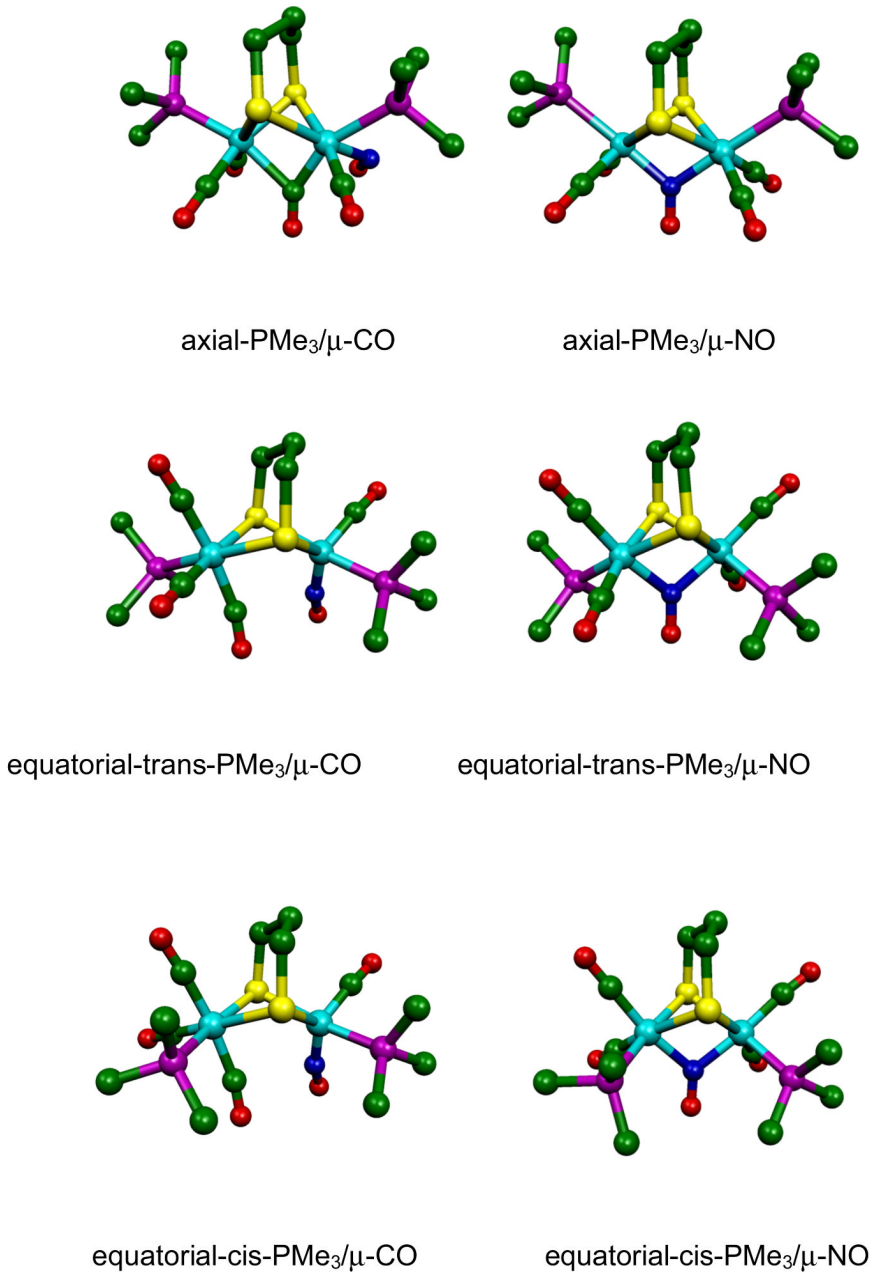

Figure 8.
DFT optimized structures of the possible isomers of **2'**CO. Atom color scheme: oxygen, red; nitrogen, blue; carbon, green; iron, cyan; sulfur, yellow; and phosphorus, purple.

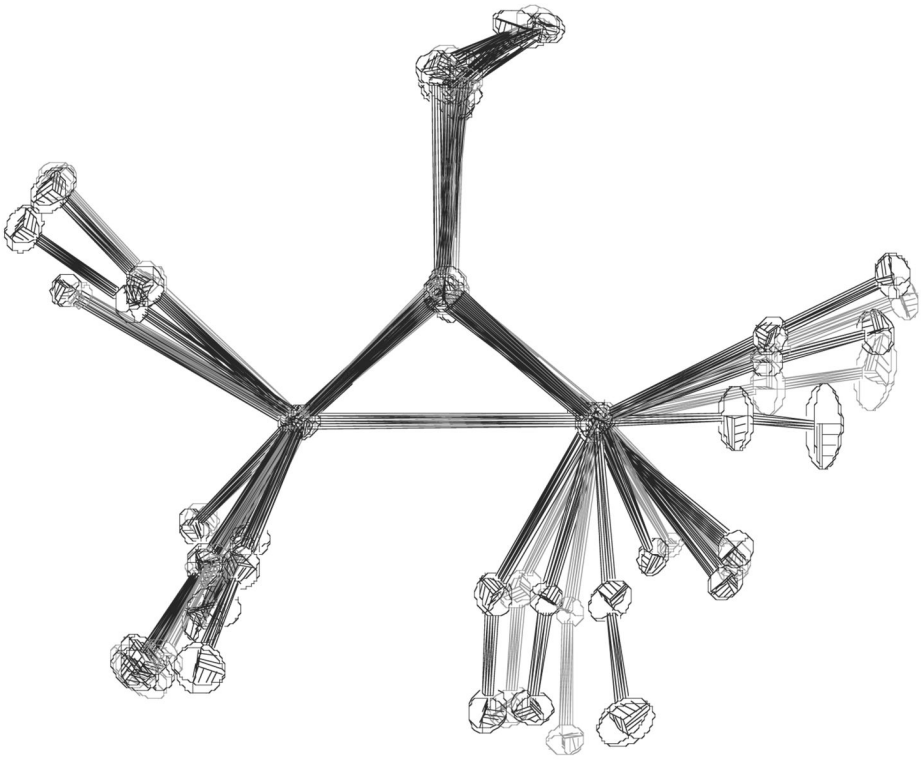

Figure 9.
Overlay of (order from left to right): **2'^{ba}** (the examples in the asymmetric unit), **2'^{ap}**, **2**, and **1** (thermal ellipsoids set at 10% and the anions; H atoms, and phosphine methyls omitted).

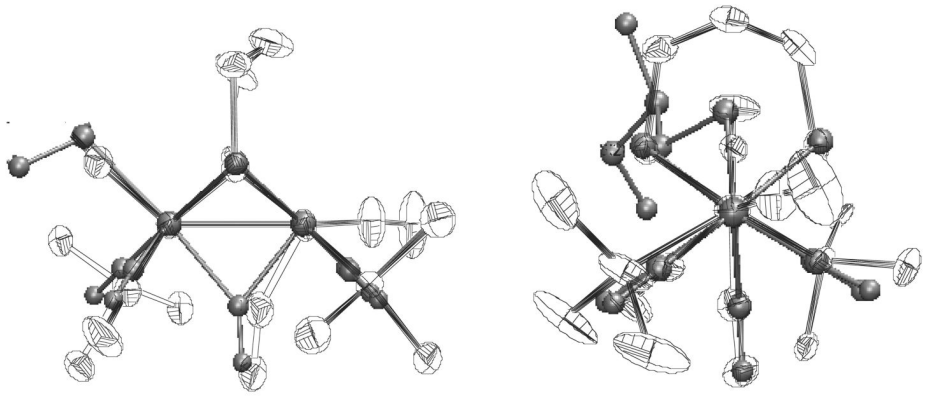

Figure 10.
Overlay of **2'^{ba}** with the diiron portion of the H_{ox} state from *C. pasteurianum*.[45] The molecule of **2'^{ba}** with a smaller Ψ value was selected.

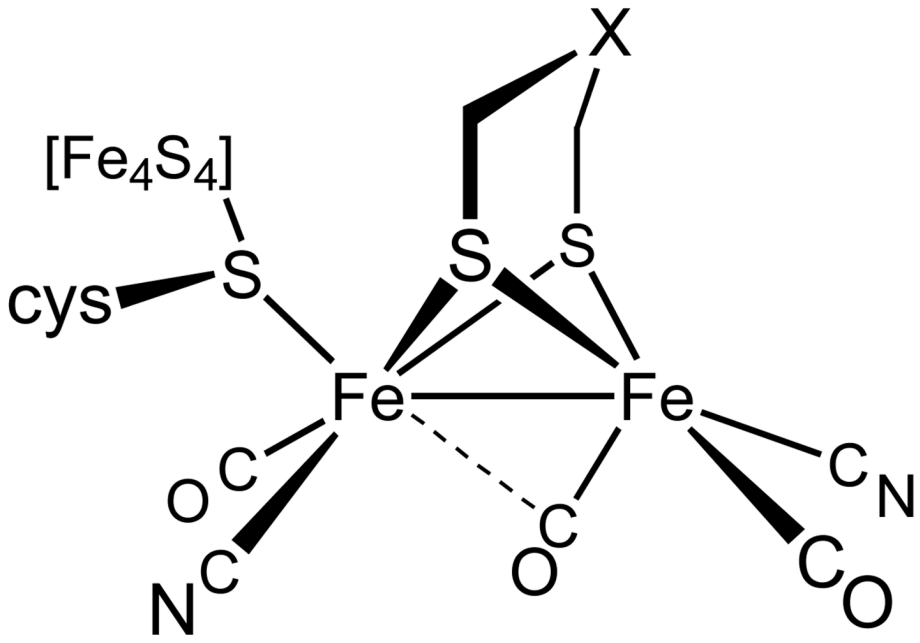

Scheme 1.
Structure of the Diiron Active Site of the [FeFe]-Hydrogenases (X = CH_2, NH, or O).

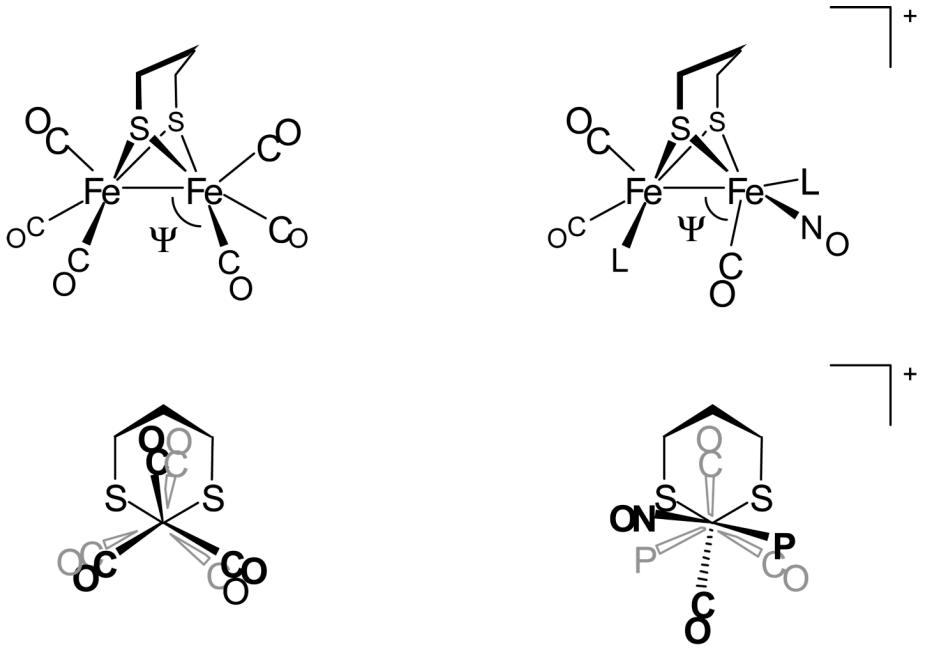

Scheme 2.

Idealized Frameworks for C_{2v} Structure (left, Fe-CO vectors twisted for clarity) and the T-Shaped Rotated Framework (right).

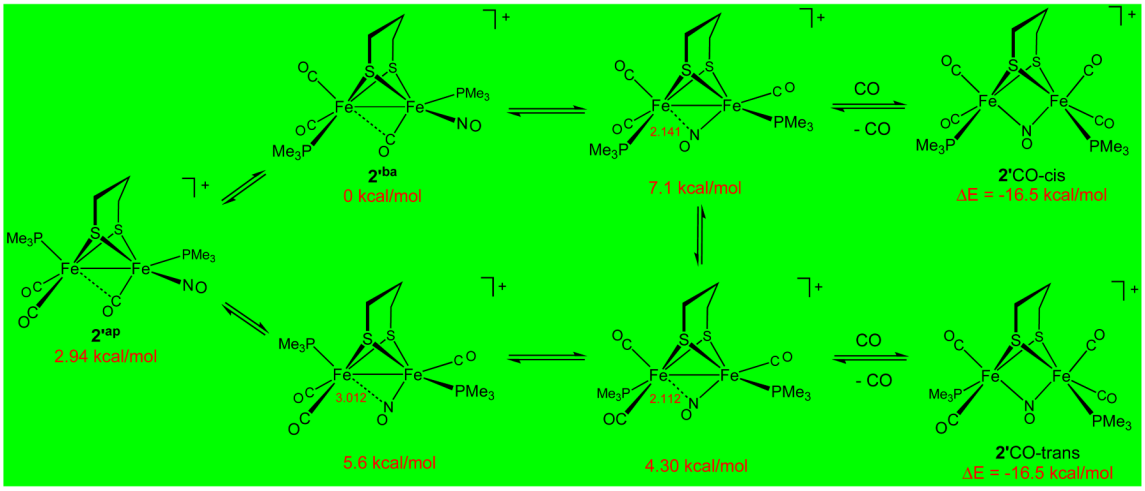

Scheme 3.
Proposed Pathways for the Carbonylation of **2'**.

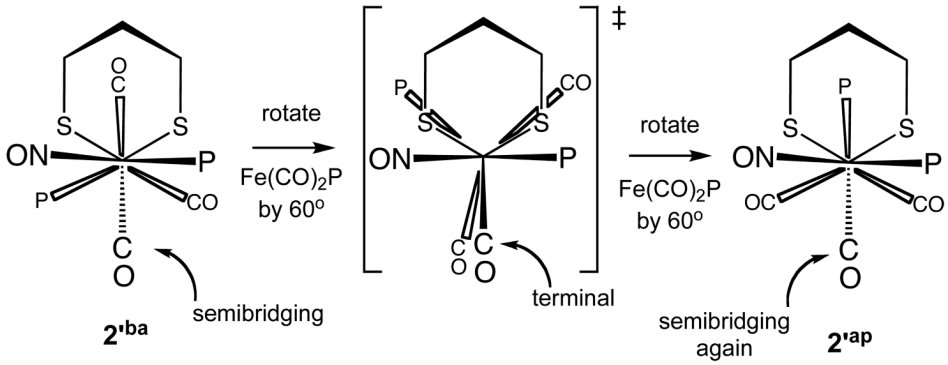

Scheme 4.
View down the Fe-Fe axis, showing the proposed pathway for interconversion of **2'ba** and **2'ap**.

Table 1

Fe-Fe-*C*O Bond Angles for Various Compounds.

Diiron dithiolate	Ψ (deg)[c]
1	91.3, 91.1
2	80.5
2'[ap]	76.1
2'[ba]	62.1, 66.6
$[Fe_2(S_2C_3H_6)(CO)_3(dppv)(PMe_3)]^+$ [a]	72.0
$[Fe_2(S_2C_3H_4)(CO)_4(iMes)(PMe_3)]^+$ [b]	56.8
$Fe_2(S_2C_3H_6)(CO)_6$ [27]	101.0
$Fe_2(S_2C_3H_6)(CO)_5(P(C_6H_5)_3)$ [28]	96.2
$Fe_2(S_2C_3H_6)(CO)_4(PMe_3)_2$	103.6
$Fe_2(S_2C_3H_6)(CO)_3$(triphos) [d]	88.3

[a] dppv is *cis*-1,2-bis(diphenylphosphino)ethene.[7]

[b] iMes is *N*,*N*'-bis(mesityl)imidazolidene.[8]

[c] The smallest Ψ value of the various carbonyls was selected.

[d] triphos is (κ^3–$Ph_2P(CH_2)_2P(Ph)(CH_2)_2PPh_2$).[29]

Table 2

Reduction Potentials (V) of **1**, **2**, **3**[a] and Related Non-Nitrosylated Derivatives

Complex	$E_{1/2}$	$E_{1/2}$
$[Fe_2(S_2C_2H_4)(CO)_4(PMe_3)(NO)]^+$	−0.45[b]	−0.95[b]
$[Fe_2(S_2C_3H_6)(CO)_4(PMe_3)(NO)]^+$	−0.36	−1.03
$Fe_2(S_2C_3H_6)(CO)_5(PMe_3)$[c,d]	−1.86	--
$[Fe_2(S_2C_2H_4)(CO)_3(PMe_3)_2(NO)]^+$	−0.67	−0.98
$[Fe_2(S_2C_3H_6)(CO)_3(PMe_3)_2(NO)]^+$	−0.64	−0.98
$Fe_2(S_2C_3H_6)(CO)_4(PMe_3)_2$[c]	−2.08	--

[a] Conditions: 1.5 mM in CH_2Cl_2, 100 mM Bu_4NPF_6, at 20 °C unless further specified, referenced versus Ag|AgCl (saturated KCl).

[b] 0 °C.

[c] In CH_3CN soln.[37]

[d] vs $Ag|AgNO_3$.[28]

Table 3

NBO Charges of **2'^{ap}**, **2'^{ba}**, $Fe_2(S_2C_3H_6)(CO)_4(PMe_3)_2$ (ap and ba isomer), and $[Fe_2(S_2C_3H_6)(CO)_4(PMe_3)_2]^+$ (ap and ba isomer) Computed at RI—BP86/def—TZVP Level of Theory.

Complex	Fe^{CO}	Fe^{NO}
2'^{ba}	−0.22	0.03
2'^{ap}	−0.19	0.03
$Fe_2(S_2C_3H_6)(CO)_4(PMe_3)_2$	−0.19 to −0.18[a]	−0.19 to −0.21[a]
$[Fe_2(S_2C_3H_6)(CO)_4(PMe_3)_2]^+$	−0.19 to −0.21[a]	−0.02 to −0.00[a]

[a]The range of values correspond to the results for different isomers (see Supporting Information).

Table 4

Vibrational Frequencies and Intensities of the **2'^{ap}** and **2'^{ba}** Computed at the RI—BP86/def—TZVP Level of Theory.

2'^{ap} ν_{NO} and ν_{CO} (rel int.)	**2'^{ba} ν_{NO} and ν_{CO} (rel. int.)**	**observed (CH_2Cl_2 soln)**
1814 (843)	1817 (795)	1787
1975 (289)	1880 (418)	
1978 (490)	1988 (532)	1981
2030 (780)	2028 (559)	2033

Table 5

Binding Energies (kcal mol^{-1}) for **2'^{ba}** + CO → **2'**CO Computed at RI-BP86/def-TZVP Level of Theory.

Reaction	Δ*E*
2'^{ba} + CO → axial-PMe_3/μ-CO	23.4
2'^{ba} + CO → axial-PMe3/μ-NO	4.3
2'^{ba} + CO → equatorial-cis-PMe_3/μ-CO	−0.3
2'^{ba} + CO → equatorial-cis-PMe_3/μ-NO	−9.4
2'^{ba} + CO → equatorial-trans-PMe_3/μ-CO	−1.6
2'^{ba} + CO → equatorial-trans-PMe_3/μ-NO	−12.2